ISSUE FOCUS ///
NITRIDING / FORGING

THE INFLUENCE OF INDUCTION HARDENING, AND BORONIZING ON CERTAIN STEELS

Based on the similarity of the physicochemical processes during nitriding and boronizing, engineers generally believe that all materials suitable for nitriding are also suitable for boronizing.

By FRANTIŠEK NOVÝ, JAKUB HARVANEC, and MILOŠ MIČIAN

eat-treatment technology changes all the mechanical properties of metallic materials. The influence of induction hardening, nitriding, and boronizing on the change in the microhardness, impact toughness, microstructure, and coefficient of friction of conventional steels 42CrMo4 and 32CrMo12 has been examined and compared with results obtained in the sintered steels with an increased content of Cu, which were prepared using powder metallurgy technology. Widely used treatments for the examined materials include induction hardening and gas nitriding. This study focuses on comparing those technologies with alternative technologies of boronizing. It was found that for powder metallurgy materials, boronizing is a much more suitable process than nitriding because after the application of nitriding, the impact toughness dropped to one third of the impact toughness of the base material, while after boronizing, the impact toughness remained unchanged. Through boronizing, it was possible to achieve the unique possibility of improving the mechanical properties of sintered PM Fe-Cu-C steels and fully replacing the currently used nitriding process. Furthermore, compared to nitriding, it also increases the hardness of the surface layer many times to improve the friction properties and significantly increases the impact toughness.

1 INTRODUCTION

Induction-hardening technologies are widely used to improve the mechanical properties of metallic materials. Induction hardening is included among many commonly used heat-treatment technologies. It involves heating the material, usually using a heating inductor, a very short dwell at the austenitizing temperature and fast cooling. Due to the skin effect, only the relatively thin surface layer of the metal is heated and hardened. This is a fast process, which is suitable for mass production. The parameters of the microstructure and mechanical properties of the induction-hardened layer are fully comparable to the material parameters obtained using traditional quenching and tempering processes. An advantage of this process is that only the thin surface layer (from 1 to 6 mm) of the treated metal is hardened, while the core of the material stays unchanged [1].

Nitriding combines heat-treatment technology with nitrogen diffusion to the material surface. Nitriding can be carried out in four different ways depending on the medium used: powder, liquid, gas, or plasma. Gas and plasma nitriding processes are most used. When gas nitriding is used, the material is heated in a special chamber filled with an atmosphere of nitrogen or ammonia. The heating temperature can be chosen in the range from 470°C to 580°C, usually above 550°C [1,2,3]. The temperature dwell varies by the type of used atmosphere and the required thickness of the diffused layer. The diffusion rate is very low, and the nitriding times are very long. The typical thickness of the nitride layer obtained on conventional steels by gas nitriding after 20 hours is usually about 300 µm. The production of thicker layers is uneconomical and technically demanding. Nitriding in an atmosphere with higher pressure can increase the diffusion rate

[4]. The hardness of the diffused nitride layer can reach 1200 HV [1,4].

The boronizing process is a surface diffusion treatment analogous to nitriding or carburizing. The only difference is that instead of nitrogen or carbon, the boron is diffused into the material surface [5,6]. Also, the boronizing can be carried out in either a gas, molten salt, or pack media. Currently, it is a very rarely used technology that is not usually used in mass production, and therefore, the most used is pack boronizing, because it is fast, simple, and low cost [7]. The boronizing temperature can be chosen from 850 to 1,050°C, depending on the type of material being processed [5,6,8,9,10,11]. The diffusion rate is even slower than in the case of nitriding, and it is only 0.02 mm per hour. The diffusion time varies by the temperature and required thickness of the boronized layer in the range from 2 to 10 hours [5,7,8,10]. The thickness of the boronized layer is usually in the range of 20 to 100 µm. This is caused by the slow diffusion rate, as mentioned before. For example, Mei et al. obtained a boronized layer with a thickness of 70 µm [12]. However, a higher thickness of the layer can be obtained, but it is time consuming and expensive [11]. The hardness of the diffused layer after boronizing is usually in the range of 1,200-2,000 HV [9,11,12,13].

Many current studies have tried to improve the diffusion rate of the boronizing process. As Mei et al. [12] reported, the diffusion rate can be improved by adding rare earth CeO₂ or Cr₂O₃. It also improves the microhardness, microstructure, and wear resistance of the boride layer. As the results showed, the optimal amount of rare earth content for the boronizing of H13 steel is about 4% [12].

Due to the boron diffusion into the Fe lattice, the formation of two kinds of borides, FeB and Fe2B, is permitted [5,9,14,15]. A layer of borides can be two-phased (FeB + Fe $_2$ B) or mono-phased (Fe $_2$ B). In high-alloy steels, the content of the FeB phase in two-phase layers can reach 50% [14,16]. These two phases have different thermal expansion coefficients so that cracking can occur at their interfaces [14,17]. These two phases also have different hardnesses. The hardness of the FeB phase is usually about 2,000 HV, while the hardness of the Fe2B phase is usually in the range of 1,200 to 1,600 HV [9,10,13]. Osman Yilmaz et al. [13] obtained the microhardness of the boride layer on AISI 4140 steel in the range from 1,600 to 1,850 HV 0.1.

From the results by Kusmanov et al. [18], there is also a presumption for the decrease in the coefficient of friction after applying the boronizing process. In their case, boronizing was combined with nitrogen and carbon diffusion. The coefficient of friction (COF) went from COF = 0.16 in non-treated conditions to COF = 0.11 for samples boronitrocarburized at 850°C for 5 minutes.

It is also known that the resistance to dry sliding of boronized specimens is better than the resistance of specimens treated by alternative surface treatment, for example, gas nitriding [19]. As proven in Lou et al.'s research [20], the boronized layer is not only wear-resistant but also corrosion-resistant at high temperatures [11.20.21.22.23].

The nitriding and boronizing of conventional steels have been

studied in considerable detail and used in technical practice for many years [24]. Recently, more metal parts with complex shapes are being produced using powder metallurgy (PM), because PM components usually achieve their final geometry without the need for machining, and their mechanical performance reaches a similar level as fully dense wrought steel. Many PM steels are used in conditions of intense friction and high-contact pressures. Therefore, there is a need to increase their surface hardness and abrasion resistance using various technologies. Copper PM steels are especially considered the backbone material of the PM industry. Their overall usage surpasses other PM material systems. The versatility and cost-effectiveness of PM iron-copper-carbon steels make them the preferred alloy system for numerous applications [25]. In addition to surface treatments such as PVD or thermal spraying, chemical-thermal treatments, such as nitriding, can also be applied to PM steel parts. Furthermore, nitrided PM Fe-Cu-C steel components have demonstrated reliable performance in certain machines. While the hardness of nitride layers on PM Fe-Cu-C steels is relatively high, some specialized applications still require further improvement. Therefore, this study investigates the feasibility of boronizing PM Fe-Cu-C steels and conducts a comprehensive comparison of the results obtained from induction hardening, nitriding, and boronizing on both conventional and PM Fe-Cu-C steels.

2 MATERIALS AND METHODS

Four different materials (2 conventional steels 42CrMo4 and 32CrMo12 and 2 experimental PM Fe-Cu-C steels) were used as experimental

Chemical compositions of 42CrMo4 steel and 32CrMo12 steel are shown in Table 1 and Table 2. These conventional steels were chosen as a reference material with a long-standing history of successful application in nitrided components. 42CrMo4 steel provides a unique combination of strength and toughness, making it an optimal material for heavily loaded automotive components such as gears, axles, and shafts. A common heat-treatment process for this steel involves quenching and tempering (Q&T) followed by nitriding. The steel was supplied in the Q&T condition (hardened at 850°C with oil quenching and tempered at 560°C), achieving a tensile strength of 980 MPa (300 HV10). 32CrMo12 steel is used in automotive components, which requires high hardness and wear resistance. Categorized as a nitriding steel, it was also delivered in the Q&T condition (hardened at 910°C with oil quenching and tempered at 630°C), resulting in a tensile strength of 1070 MPa (330 HV10). According to the material certificate, nitriding in the temperature range of 480-570°C should reach a nitride layer hardness between 480 and 570 HV1 on 32CrMo12 steel.

С	Si	Mn	P	S	Cr	Mo	Fe
0.38-0.45	Max. 0.4	0.6-0.9	Max. 0.025	Max. 0.035	0.9-1.2	0.15-0.3	Balance

Table 1: Chemical composition of 42CrMo4 steel (in wt. %) [26].

С	Si	Mn	P	S	Cr	Mo	Ni	Fe
0.28-0.35	Max. 0.4	0.4-0.7	Max. 0.035	Max. 0.035	2.8-3.3	0.3-0.5	Max. 0.6	Balance

Table 2: Chemical composition of 32CrMo12 steel (in wt. %) [27].

Specimen	Cu	С	Density [g·cm ⁻³]
PM1	1.8	0.75	7.1
PM2	4.0	0.60	7.0

Table 3: Chemical composition of the experimental PM Fe-Cu-C steels (in wt. %).

Experimental PM Fe-Cu-C steels, labelled as PM1 and PM2, were not normalized. Both belong to the excellent universal grade group offering high wear resistance, high strength, and good shock load capacity. These steels can be used with or without heat treatment and were produced according to ASTM B783-04 and ASTM B783-93 standards.

According to MFIP Standard 35 [28], PM1 material is equivalent to sintered FC-0208-95HT copper steel, and PM2 material is equivalent to sintered FC-0205-90HT copper steel. A premix Fe-Cu-C, conforming to SINT C/D11, was used. Compaction was performed using a mechanical press and by sintering in an Abbott belt furnace at 1,125°C for 30 minutes in a 90% H₂/10% N₂ atmosphere. Subsequent tempering was conducted at 180°C for 30 minutes. The sintered density of the compacts is given in Table 3.

It is well known that sintered dimensional change and shrinkage during the sintering of PM Fe-Cu-C steels are influenced by several factors, including the amount and type of premixed copper, the amount of graphite in the premix, particle size, particle distribution, green part density, and sintering conditions. These influences have been extensively studied [29,30]. This study focuses solely on the influence of the substrate type on the quality of the boronized layer. The influence of the chemical composition of PM on dimensional stability is beyond the scope of this study.

PM Fe-Cu-C steels typically contain higher levels of carbon (>0.5%) to achieve similar strengths as wrought products. The copper forms a liquid during sintering and infiltrates into the fine pores, where it later diffusionally solidifies, thereby increasing the volume of sintered necks in the compact. The chemical composition of the sintered steels PM1 and PM2 are given in Table 3. In addition to the chemical elements listed in Table 3, the metallic powder also contains 0.9% of lubricants and binders. These additives improve pressability and prevent the powder from sticking to the surface of the press mold during the manufacturing process.

First, semi-finished products were obtained from each experimental material to produce final specimens. For conventional steels, a 20 mm diameter round bar served as the starting material. Rectangular blocks measuring $10 \times 10 \times 115$ mm, suitable for tribological and impact toughness tests, were milled from these bars. Similarly, rectangular blocks of the same dimensions were produced from the sintered steels using powder metallurgy techniques, ensuring a dimensional accuracy of ±0.1 mm.

The rectangular blocks were then used to produce specimens for tribological and impact toughness tests. For tribological tests, the rectangular blocks were ground under identical conditions to achieve comparable surface roughness. Specimens made from conventional steels achieved a surface roughness of Ra = 0.8 µm after grinding,

while PM steels, due to their inherent porosity, exhibited a higher surface roughness of $Ra = 1.6 \mu m$. For the impact toughness tests, the standard specimens of dimensions 10 \times 10 \times 55 mm were cut from semi-finished rectangular blocks with a dimensional accuracy of ±0.1 mm and surface roughness of up to Ra = 3.2 μm. Conventional steel specimens required a U-notch with a 1 mm root radius and a 2 mm depth to enhance fracture using a Charpy pendulum with a nominal impact energy of 300 J, as these steels exhibit relatively high impact strength after induction hardening. In contrast, PM specimens were tested as smooth blocks without a notch due to their naturally higher brittleness. The Charpy test specimens were manufactured in accordance with the recommendations of the EN ISO 148-1: 2011 standard with the exception of the smaller U-notch depth. This deviation, justified by historical practice and previous standard versions, is still employed in specific cases.

After machining, all specimens were divided into three groups and subsequently surface hardened using three different technologies: namely, induction hardening, gas nitriding and pack boronizing.

The first group of specimens underwent induction hardening at a temperature range of 1,000-1,050°C. The induction hardening process parameters were set as follows: electric power of 42 kW, frequency of 167 kHz, voltage of 133 V, current of 31 A, a dwell time of 0.6 seconds, and an inductor feed rate of 1,100 mm/min. After induction hardening, the specimens were two-stage tempered. First, they were tempered for 1 hour at 80°C; then, they were heated to 150°C for 1 hour, which was followed by air cooling. This two-stage tempering process is commonly used in the mass production of induction-hardened parts made from conventional steels such as 42CrMo4 or 32CrMo12.

The second group of specimens was subjected to gas nitriding. The nitriding atmosphere consisted of $NH_3 + N_2$, the temperature was set to 575°C, the nitriding duration was 4 hours, and the specimens were cooled slowly within the nitriding furnace.

Finally, the third group of specimens underwent pack boronizing. At first, the technological parameters were set to a temperature of 850°C, a boronizing duration of 6 hours, and slow cooling in the furnace. However, microstructure examination revealed that the resulting boronized layer was unsatisfactory, being too thin and poorly bonded to the substrate. After consulting with a heat-treatment specialist, the technological parameters were adjusted to a temperature of 1,000°C, a boronizing duration of 6 hours, and slow cooling in the furnace, which was followed by re-hardening (austenizing at 850°C for 2.5 hours in a vacuum furnace with subsequent oil quenching in an Ar atmosphere) and tempering at 150°C for 2 hours.

By increasing the boronizing temperature, it was possible to achieve a high-quality boronizing layer that perfectly bonded to the substrate.

The rectangular shape of specimens imitates the complex shapes of PM components in practical applications, where corners are prone to overheating during induction hardening and oversaturation during nitriding and boronizing. However, metallographic analysis revealed the chosen technological parameters for induction hardening, nitriding, and boronizing were optimal, preventing oversaturation.

After heat-treatment procedures, tribological tests, impact toughness tests, microhardness tests, microstructure analysis, and microchemical analysis using energy-dispersive spectroscopy (EDX) were conducted.

3 RESULTS

3.1 Tribological Test

For tribology tests, a ball-on-plate reciprocating friction system was used. A standard test method for linearly reciprocating ball-on-plate sliding wear (ASTM G133-22) was used. During this test, a 100Cr6 bearing steel ball undergoes linear reciprocal motion on the tested material under a load of 10 N. The direction of relative motion between sliding surfaces reverses periodically, resulting in back-and-forth straight-line sliding. The moving speed of the ball was set to 20 mm/min, leading to a total travel distance of 100 m over a 6,000-s testing period. Experiments were performed at the temperature of $22 \pm 2^{\circ}$ C under dry friction conditions in open air.

Three tribological tests were conducted for each specimen group, and the resulting average coefficients of friction and standard deviations were incorporated into Table 1.

Surface hardening brought rather surprising results in terms of changes in the coefficient of friction. As can be seen in Figure 1, induction hardening and nitriding did not significantly change the coefficient of friction in conventional steels. Their impact was more pronounced on PM Fe-Cu-C steels, which was primarily due to changes in porosity influenced by process parameters, especially temperature. Compared to nitriding, boronizing significantly reduced the coefficient of friction in both conventional and sintered steels. Boronizing emerges as a particularly suitable surface-hardening technology for PM steels, which is capable of producing very hard layers with low friction coefficients. However, a major disadvantage of the boronizing process is the need for the re-hardening of the substrate, the hardness of which drops sharply due to undesirable phase transformations occurring at high boronizing temperatures.

3.2 Impact Toughness Test

Impact toughness tests were performed using a Charpy pendulum with a nominal impact energy of 300 J and a striker with a 2 mm tip radius. The testing temperature was maintained at $22\pm2^{\circ}C$. The absorbed energy was measured for both U-notched conventional steel specimens and smooth PM Fe-Cu-C specimens. The data were then converted into deformation work consumed per unit area of fracture (impact toughness in J/cm²) by dividing the absorbed energy by the actual cross-sectional area of the specimen. U-notches with a depth of 2 mm were introduced into the conventional steel specimens before heat treatment. The cross-section for these specimens was calculated according to a more precise, older version of the STN EN ISO 148-1 to account for the notch. Specimens of PM Fe-Cu-C steels were tested without notches.

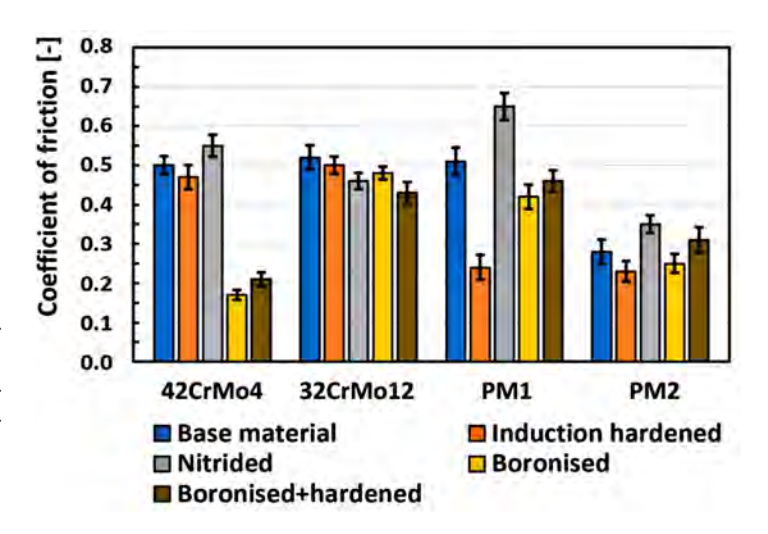


Figure 1: Comparison of coefficient of friction of experimental steels (42CrMo4, 32CrMo12, PM1 and PM2) before and after surface hardening; reciprocating ball-on-plate sliding.

Three Charpy pendulum tests were conducted on each specimen group, and the average impact toughness values with standard deviations are shown in Figure 2 and Figure 3.

Nitriding is frequently used as an optional heat-treatment process for conventional 42CrMo12 steel. As can be seen in Figure 2, nitriding can significantly increase the impact toughness of 42CrMo12 steel. An increase in the impact toughness after nitriding is generally attributed to the positive influence of molybdenum.

On the other hand, it is evident that using nitriding can also cause a significant decrease in the impact toughness of other conventional and PM steels. In this study, the impact toughness of 32CrMo12 steel

decreased by half after nitriding. Furthermore, the impact toughness of PM Fe-Cu-C steels was reduced by as much as one third following nitriding.

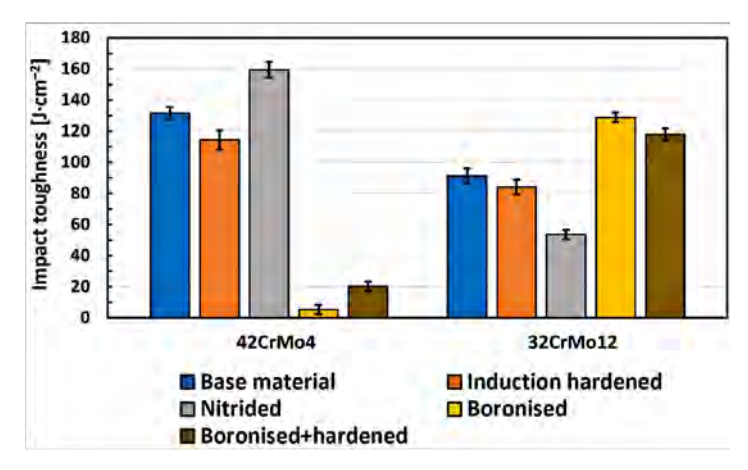


Figure 2: Comparison of impact toughness of conventional steels 42CrMo4 and 32CrMo12 before and after surface hardening.

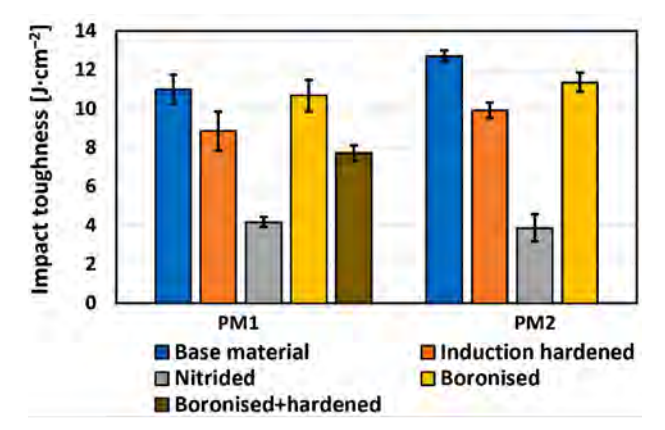


Figure 3: Comparison of impact toughness of experimental PM Fe-Cu-C steels – PM1 and PM2 before and after surface hardening.

During nitriding and boronizing, the surface layers of steel are saturated with interstitial atoms of nitrogen and boron. The diffusion processes occurring during nitriding and boronizing are analogous, but they are also very different due to the distinct structural changes induced in the processed steel, which makes comparing nitriding and boronizing very difficult. Conventional steels are typically nitrided in the quenched and tempered (Q&T) condition. The industrial nitriding of Q&T steels is typically performed within a process-dependent temperature range of 350-600°C, which is preferably between 550 and 580°C. Higher process temperatures facilitate deeper nitrogen penetration within the material for a given treatment time. However, higher temperatures and prolonged holding times also promote microstructural changes within the Q&T steel substrate, leading to a reduction in its hardness.

The nitriding of steels generally occurs below the high-temperature tempering range (350-700°C), preventing solid-state phase transformations such as the transformation of ferrite, pearlite, or martensite to austenite. Only the transformation of martensite to sorbite may occur. In contrast, boronizing typically occurs above the transformation temperature, leading to the saturation of the steel surface with boron within the austenitic phase. These solid-state phase transformations result in significant microstructural changes within the steels during boronizing. These microstructural changes significantly affect the mechanical properties of the boronized steels.

Therefore, to restore the original sorbitic microstructure of the Q&T steel, re-hardening (quenching and tempering) after boronizing is necessary. However, some negative effects, such as grain coarsening during prolong austenitizing at high temperatures and detrimental changes in segregation, are irreversible. These effects, along with other diffusion-related changes within the solid solution of the metal matrix, contribute to significant embrittlement. In the case of 42CrMo steel, extensive negative microstructural changes occurred during boriding, leading to complete embrittlement. The irreversible nature of these changes in 2CrMo steel is so pronounced that even re-austenitization followed by rapid cooling failed to restore its impact toughness to more than one fifth of its original level before boronizing.

Contrary, in 32CrMo12 steel, nitriding resulted in a decrease in the impact toughness. This is likely attributed to the use of a slightly elevated nitriding temperature (approximately 5°C above the recommended range) for all experimental steels. However, unexpectedly, boronizing led to a significant increase in the impact toughness of 32CrMo12 steel.

PM Fe-Cu-C steels can be used with or without heat treatment. Therefore, some specimens were solely boronized to achieve a relatively soft, pearlitic microstructure, while others were boronized, hardened, and tempered to attain a hard, sorbitic microstructure. Recognized for their inherent brittleness, the practical applications of PM Fe-Cu-C steels are somewhat limited. As illustrated in Figure 3, induction hardening or hardening and nitriding further exacerbated the brittleness of these steels. Conversely, these experiments demonstrated that both PM Fe-Cu-C steels can be boronized without significantly compromising their impact toughness. Re-hardening the boronized PM Fe-Cu-C steels, however, resulted in a marked increase in brittleness.

3.3 Microhardness Tests

Microhardness measurements were performed on the cross-sections of the surface-hardened specimens using the Vickers method (HV 0.01). Prior to testing, specimens were prepared following standard metallographic procedures. This involved sectioning, mounting in a hard compression powder using a press, and subsequent mechanical grinding and polishing. An electrically conductive polishing powder was used to enable subsequent analysis using techniques such as energy-dispersive X-ray spectroscopy (EDX) in an electron microscope. After preparation, microhardness measurements were gained using an automated microhardness tester under an applied test force of 0.01 kgf (0.098 N).

Regarding the influence of surface-hardening technology on the achieved hardness and layer thickness, the measured hardness after the induction hardening and nitriding of 42CrMo4 and 32CrMo12 steels correspond to the typical values observed in industrial practice.

After the boronizing of 42CrMo4 and 32CrMo12 steels, the measured hardness increased more than four times compared to the values achieved after nitridation; see Figure 4 and Figure 5. This study successfully produced a compact, extremely hard boride surface layer on these steels. This layer exhibited excellent adhesion to the substrate and significantly exceeded the hardness and thickness of boronized layers reported by other authors [13]. The boride layer demonstrated a sharp boundary, and the diffusion zone was extremely narrow. As a result, the hardness decreased sharply from the maximum value at the surface to the substrate hardness within approximately 200 μm . Unlike the nitride layer, which exhibits a wide transition diffusion zone characterized by a gradual hardness decrease, the extremely narrow transition diffusion zone of the boronized layer cannot be accurately identified using conventional microhardness testing. For

detailed mapping of this transition zone, techniques such as nanoindentation should be used.

Re-hardening after boronizing increased the hardness of the bulk material and within the transition diffusion zone while slightly decreasing the hardness of the boride layer itself. It can be seen that re-hardening slightly increased the thickness of the boronized layer at the expense of a minor reduction in microhardness.

Surface hardening brought similar results for PM Fe-Cu-C steels. As can be seen in Figure 6 and Figure 7, induction hardening proved to be a highly suitable technology for these materials. Nitriding, however, demonstrated the least effectiveness among the applied methods. The most favorable results were obtained with boronizing either alone or followed by re-hardening.

3.4 Microstructure Analysis

Metallographic analysis was performed on the same specimens used for the microhardness tests. The microstructure was revealed by

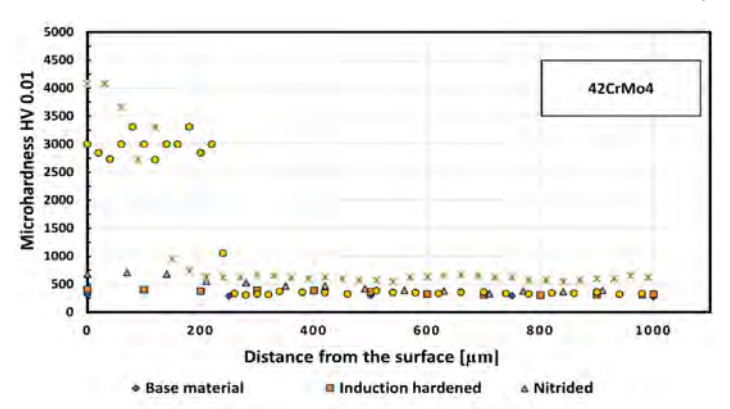


Figure 4: Microhardness of conventional steel 42CrMo4 after surface hardening.

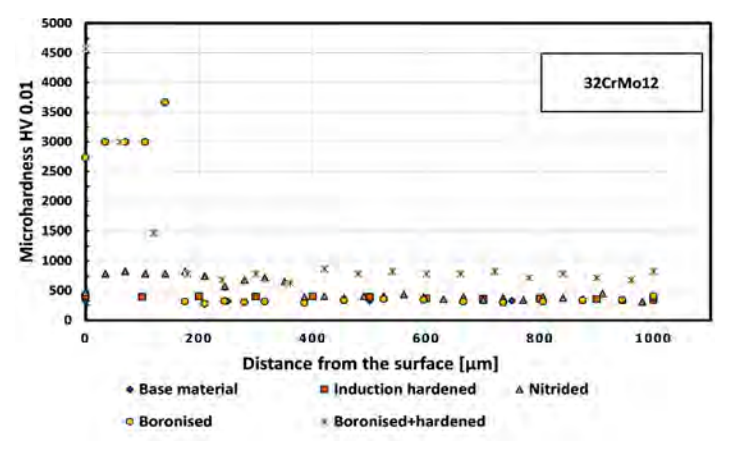


Figure 5: Microhardness of conventional steel 32CrMo12 after surface hardening.

immersion etching in 2% Nital. The analysis focused on key microstructural criteria, including the microstructure and depth of the hardened layer bond integrity between the layer and the substrate within the transition diffusion zone and microstructural changes occurring in the bulk of the experimental steels after surface hardening (induction hardening, nitriding, boronizing and re-hardening).

The microstructure of 42CrMo4 steel in the as-received (Q&T) condition, as depicted in Figure 8a, consisted of sorbite with localized regions of partially transformed coarse martensitic plates and a small amount of residual austenite. This microstructure remained identical after induction hardening.

Figure 8b illustrates the nitride layer and the sorbitic microstructure of nitrided 42CrMo4 steel. The visible thickness of the nitride layer is approximately 100 μ m, while microhardness testing indi-

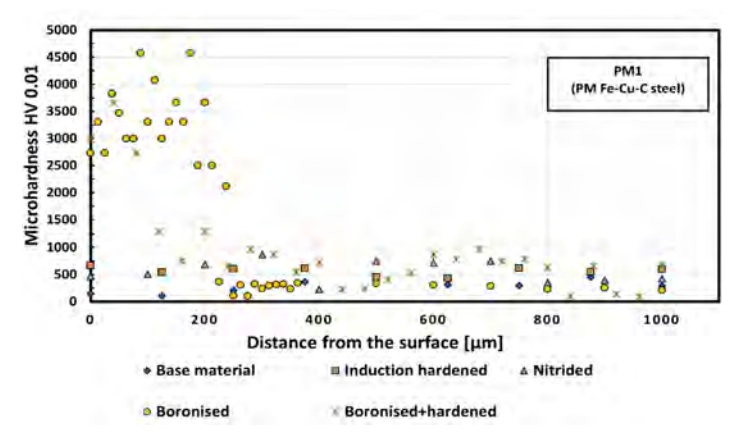


Figure 6: Microhardness of PM1 steel after surface hardening.

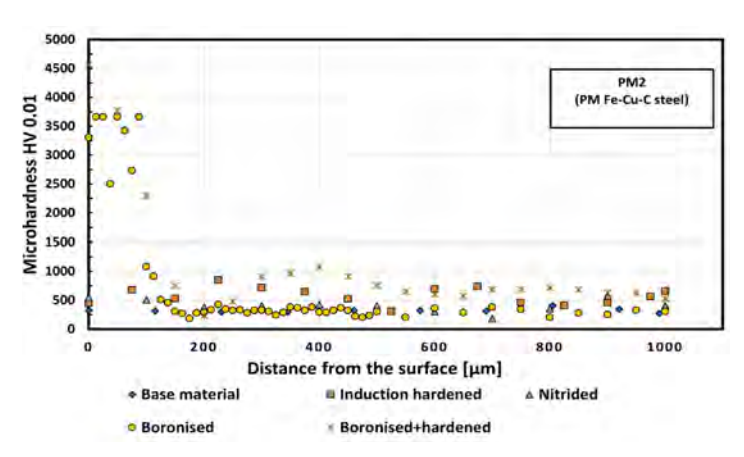


Figure 7: Microhardness of PM2 steel after surface hardening.

cates a diffusion layer depth of approximately 350 μ m. Beyond this depth, the hardness decreases due to the declining nitrogen content, as confirmed by EDX analysis (Figure 9). The substrate microstructure exhibited a finer grain size due to the transformation of coarse martensitic plates into fine sorbite during the prolonged exposure to the nitriding temperature, which is close to the high-temperature tempering temperature range for this steel.

Figure 10a depicts a detail of the sharply defined, white boride layer (approximately 150 μm thick) on the surface and reveals unfavorable microstructural changes within the diffusion zone of

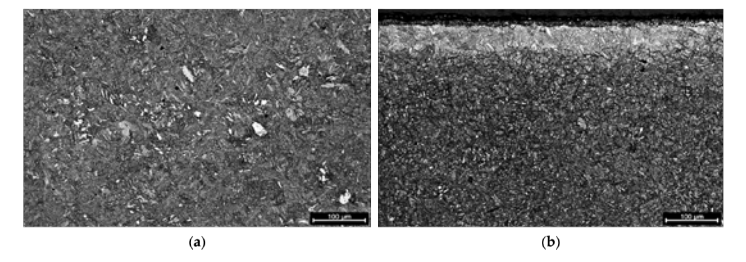


Figure 8: Microstructure of 42CrMo4 steel after nitriding: (a) sorbitic microstructure of base material in Q&T condition, (b) nitride layer, transit zone and sorbitic microstructure in the bulk; etched by 2% Nital.

the boronized 42CrMo4 steel. The prolonged exposure to the high boronizing temperature resulted in the transformation of the sorbitic microstructure to austenite, which subsequently transformed into a relatively coarse pearlitic microstructure during slow cooling. This pearlitic microstructure is primarily confined to the transition diffusion zone immediately beneath the white boride layer, where boron has been substituted for carbon. Within this narrow transition zone, a tendency toward the formation of a boride network along

grain boundaries is also evident. As shown in Figure 10b, the bulk of the substrate exhibits a pearlitic–ferritic microstructure, which is characteristic of this hypoeutectic steel in the annealed condition.

EDX analysis (Figure 11) confirmed the sharp interface observed between the boride layer and the substrate during metallographic examination. Figure 12 illustrates the boronized layer of 42CrMo4 steel after re-hardening. Re-hardening, conducted uniformly at identical process parameters for all re-treated specimens in a vacuum furnace followed by oil quenching in an argon atmosphere, resulted in significant microstructural changes. The microstructure within the transition diffusion zone and the bulk material transformed completely to a sorbitic structure. Notably, the sharply defined white boride layer on the surface remained unaffected by the re-hardening process. However, within the narrow transition diffusion zone, a boride network formed along the grain boundaries.

The sorbitic microstructure of 32CrMo12 steel in the as-received (Q&T) condition is shown in Figure 13a. Similar to 42CrMo4 steel, the microstructure remained largely unchanged after induction hardening, consisting of sorbite and residual austenite.

Figure 13b illustrates the nitride layer, transition diffusion zone, and sorbitic microstructure within the bulk of the nitride 32CrMo12 steel. The visible thickness of the nitride layer is approximately 100 μm , while microhardness testing indicates a diffusion layer depth of approximately 370 μm . Beyond this depth, the hardness decreases due to a declining nitrogen content, as evidenced in Figure 14.

Figure 15a illustrates the microstructure of boronized 32CrMo12 steel. Similar to boronized 42CrMo4 steel, a sharply defined white boride layer of approximately the same thickness is observed on the surface. The prolonged exposure to the high boronizing temperature resulted in the formation of a pearlitic microstructure, which is consistent with the phase transformations observed in 42CrMo4 steel. The primary distinction lies in the fully pearlitic microstructure within the bulk of the substrate, which is attributable to the higher chromium and nickel content of 32CrMo12 steel. The thickness of the white boride layer varies between 150 and 200 μm , and the transition diffusion zone remains narrow.

Figure 15b depicts the sorbitic microstructure of boronized 32CrMo12 steel after subsequent quenching and tempering. Similar to the as-boronized specimen, the borides exhibit a tendency to form a network along grain boundaries within the narrow transition diffusion zone. A small crack was observed within the boride layer, suggesting a need for optimization of the re-hardening parameters for this steel. Consistent with the observations in 42CrMo steel, EDX analysis (Figure 16) confirmed the sharp interface between the boride layer and the substrate.

The phase description of surface-hardened PM Fe-Cu-C steels is extremely complicated, and it will be a subject of further research. The microstructure of the PM1 steel is shown in Figure 17a, while Figure

17b shows the microstructure of the induction hardened PM1 steel.

The comparison of microstructures in Figure 17a and Figure 17b reveals a significant transformation in the surface layer of PM1 steel following induction hardening. A distinct hardened layer, approximately 1.5 mm thick, is observed, which is accompanied by a transition zone extending up to 2.4 mm from the surface. The presence of larger pores within the microstructure after induction hardening is visible. The formation of these larger pores is undesirable, as they can act as stress concentrators, potentially reducing the material's ductility and increasing its susceptibility to brittle fracture.

Figure 18a reveals the microstructure of nitriding PM1 steel. A prominent feature is the surface layer, which is enriched with nitrogen to a depth of 1.5 mm. This is followed by a transition zone extending up to 2.5 mm. Within this zone, nitrogen diffused into

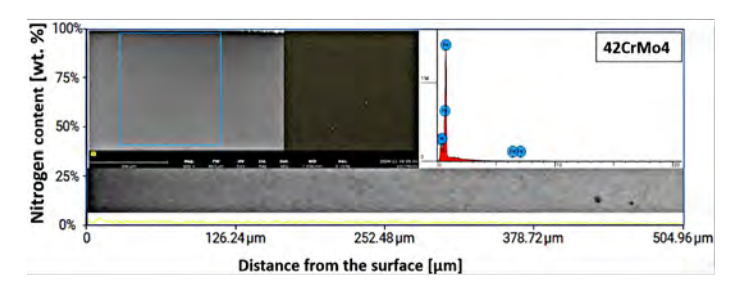


Figure 9: EDX analysis of nitriding layer in 42CrMo4 steel.

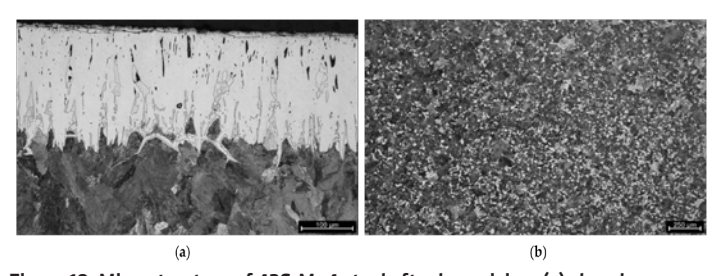


Figure 10: Microstructure of 42CrMo4 steel after boronizing: (a) sharply bounded white layer of borides and pearlitic microstructure in transit diffusion zone, (b) pearlitic-ferritic microstructure under the diffusion zone; etched by 2% Nital.

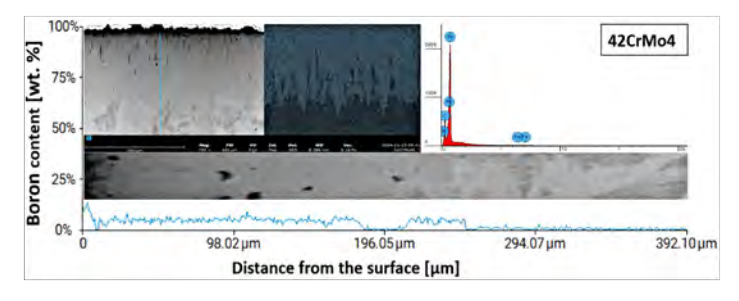


Figure 11: EDX analysis of boronizing layer in 42CrMo4 steel.

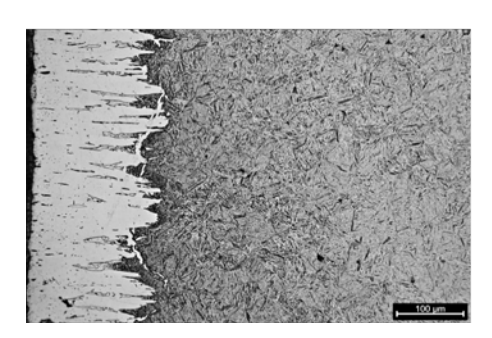
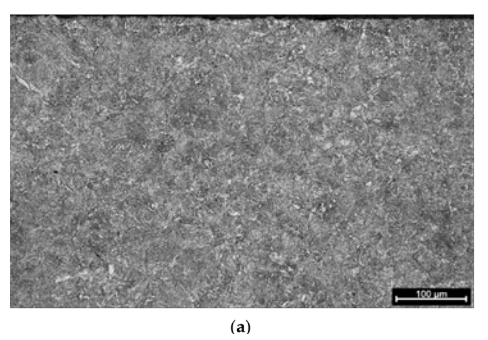


Figure 12: Sorbitic microstructure of boronized 42CrMo4 steel after quenching and tempering; etched 2% Nital.



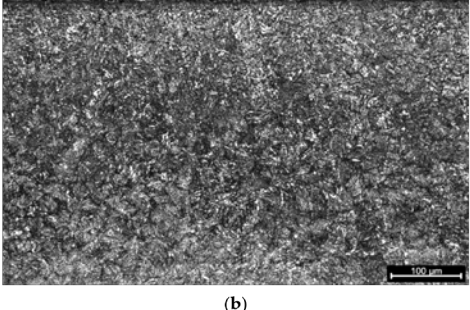


Figure 13: Microstructure of 32CrMo12 steel after nitriding: (a) sorbitic microstructure of base material in Q&T condition, (b) nitrided layer, transit zone and sorbitic microstructure in the bulk; etched by 2% Nital.

the sintered steel, notably using the existing pores to penetrate and envelop individual grains. A noteworthy observation is the presence of nitrogen supersaturation throughout the entire cross-section of the material. Beyond this, no other significant microstructural changes were observed in the nitriding PM1 steel.

High nitrogen supersaturation was also confirmed by EDX analysis (Figure 19).

Figure 18b presents the microstructure of PM1 steel following boronizing without subsequent re-hardening. The boride layer exhibits a thickness ranging from approximately 250 μ m at the center of the edge to 300-450 μ m at the corners of the specimen. Microstructural analysis revealed the presence of a single predominant boride phase

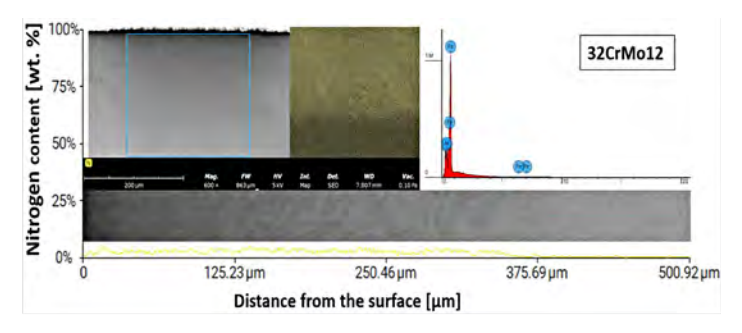


Figure 14: EDX analysis of nitriding layer in 32CrMo12 steel.

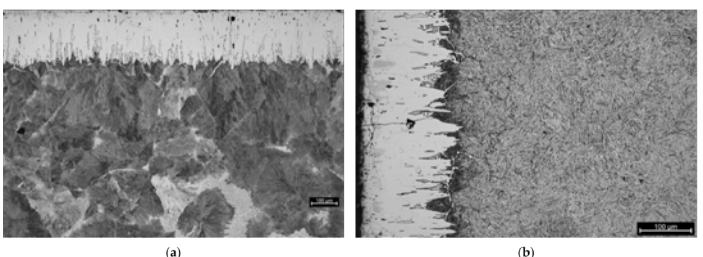


Figure 15: Microstructure of 32CrMo12 steel after boronizing: (a) sharply bounded white layer of borides and pearlitic microstructure, (b) sorbitic microstructure of boronized 32CrMo12 steel after following quenching and tempering; etched 2% Nital.

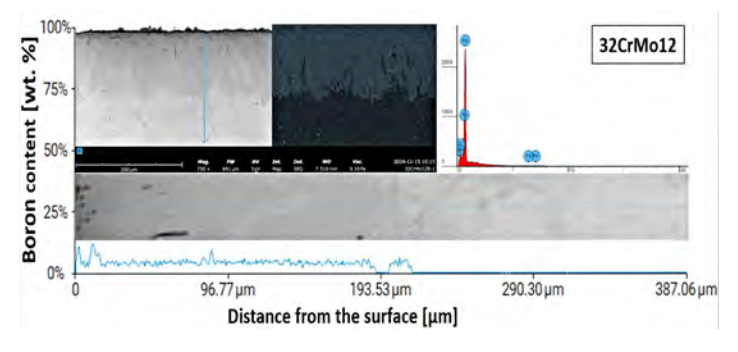


Figure 16: EDX analysis of boronizing layer in 32CrMo12 steel.

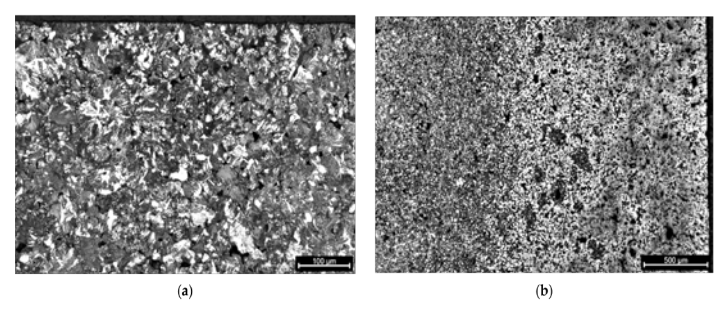


Figure 17: Microstructure of the PM1 steel, (a) base material, (b) induction hardened; etched 2% Nital.

within this layer. Based on the measured layer hardness, this phase was tentatively identified as FeB. A high density of pores was observed within the boride layer. Furthermore, a distinct transition zone was evident within the layer, which was characterized by a gradual change from the upper, white, and harder FeB phase to a lower, softer, gray phase.Boride-like formations were observed extending beyond the defined diffused layer. EDX analysis (Figure 20) confirmed that diffusion occurred deeper into the material primarily through the existing pores.

Figure 21 illustrates the microstructure of boronized PM1 steel following re-hardening. It is hypothesized that entrapped gas within the bulk material migrated toward the boride layer during the rehardening process, contributing to an increase in porosity within the boride layer (Figure 18b). The higher porosity observed in PM1 steel compared to PM2 steel was reflected in the mechanical test results. Specifically, an increase in the coefficient of friction, a slight decrease in impact toughness, and an increased scatter in the measured hardness values of the boronized layer were observed in PM1 steel.

Figure 22 illustrates the base microstructure of PM2 steel. Compared to PM1 steel, distinct differences are observed in the microstructure, including variations in the character and distribution of pores. The twice higher copper content in PM2 steel, acting as a binder for the steel powder, resulted in a significant reduction in the porosity.

Figure 23a depicts the microstructure of induction-hardened PM2 steel. The observed width of the hardened layer and the transition zone closely resemble those observed in PM1 steel, indicating minimal discernible differences between the two materials in response to this surface-hardening treatment.

Figure 23b presents the microstructure of nitrided PM2 steel. Notably, EDX analysis (Figure 24) revealed that nitrogen diffusion penetrated the entire cross-section of PM2 steel.

Figure 25a presents the microstructure of boronized PM2 steel. The boride layer exhibits a thickness ranging from 160 μ m to 200 μ m. Notably, this layer displays a higher degree of porosity compared to that observed in PM1 steel. Furthermore, the transition diffusion zone remains narrow, which is similar to that observed in PM1 steel.

Figure 25b presents the microstructure of boronized PM2 steel following re-hardening. The porosity within the boride layer and its overall thickness (ranging from 180 μm to 200 μm) remained largely unchanged after the re-hardening process. A notable observation is the appearance of small cracks within the boride layer after re-hardening, which are similar to those observed in boronized 32CrMo12 steel. This suggests a potential need for optimization of the re-hardening parameters for PM2 steel to lower the formation of these cracks. The boride layer in PM2 steel exhibits a sharp boundary, which is similar to that observed in conventional steel. Minimal boride-like formations were observed beyond the defined diffusion zone. EDX analysis (Figure 26) revealed that boron diffusion extended to a depth of approximately 150 μm within the material.

4 CONCLUSIONS

Based on the similarity of the physicochemical processes during nitriding and boronizing, engineers generally believe that all materials suitable for nitriding are also suitable for boronizing. Therefore, this study aimed to investigate the suitability of conventional steels 42CrMo4 and 32CrMo12 and powder metallurgy (PM) Fe-Cu-C steels, increasingly used in automotive applications, for both nitriding and boronizing.

The following conclusions were drawn from the research on the influence of induction hardening, nitriding, boriding, and re-hardening on the mechanical properties of conventional and PM Fe-Cu-C steels.

>> Induction hardening, nitriding, and boronizing can effectively enhance the mechanical properties of conventional steels. However, high-temperature boronizing of certain steels, such as 42CrMo4, can lead to irreversible embrittlement of the substrate. For 32CrMo12 steel, boronizing followed by hardening and tempering effectively improves impact toughness and hardness. Furthermore, nitriding represents the most suitable surface-hardening technology for 42CrMo4 steel.

>> Induction hardening emerged as a suitable surface hardening technology for PM Fe-Cu-C steels, effectively increasing the surface hardness and reducing the coefficient of friction while minimally affecting the impact toughness.

>> The nitriding of PM Fe-Cu-C steels proved ineffective, leading to a slight increase in hardness while deteriorating frictional properties and significantly reducing impact strength.

>> Boronizing demonstrated significant potential for enhancing the mechanical properties of PM Fe-Cu-C steels, offering a viable alternative to nitriding. Boronizing effectively increased the surface hardness, improved the frictional properties, and notably enhanced the impact toughness.

>> The hardness of experimentally obtained boronized layers significantly surpassed those reported by other authors, which was likely attributed to a higher content of the harder FeB phase within the boronized layer.

>> Based on the obtained results, it can be stated that the re-heating after boronizing should be used to increase the hardness of the substrate.

REFERENCES

- [1] Totten, G.E.; Howes, M.A.H. Steel Heat Treatment Handbook; CRC Press: Boca Raton, FL, USA, 1997.
- [2] Wang, H.; Teeter, G.; Turner, J.A. Modifying a Stainless Steel via Electrochemical Nitridation. J. Mater. Chem. 2011, 21, 2064.
- [3] Zhao, Q.; Luo, H.; Pan, Z.; Wang, X.; Cheng, H.; Zong, Y. Effect of Ion Nitriding on Properties of High Carbon Chromium Bearing Steel Containing Rare Earth Elements. J. Mater. Eng. Perform. 2023, 33, 6930-6941.
- [4] Wang, B.; Sun, S.; Guo, M.; Jin, G.; Zhou, Z.; Fu, W. Study on Pressurized Gas Nitriding Characteristics for Steel 38CrMoAIA. Surf. Coat. Technol. 2015, 279, 60-64
- [5] Keddam, M.; Kulka, M.; Makuch, N.; Pertek, A.; Małdziński, L. A Kinetic Model for Estimating the Boron Activation Energies in the FeB and Fe2B Layers during the Gas-Boriding of Armco Iron: Effect of Boride Incubation Times. Appl. Surf. Sci. 2014, 298, 155-163.
- [6] Wang, D.; Tian, H.; Zhang, X.-L.; Pang, D. The Effect of Temperature and Time on Microstructure and Friction Performance of RE-Borosulphurizing Composite Coatings. Surf. Coat. Technol. 2018, 344, 722-728.
- [7] Ocak-Araz, S.; Birden, A.; Bayca, S.U.; Bican, O. Effect of Powder-Pack Boronizing on the Microhardness, Wear, and Corrosion Behaviors of AISI 304L Steel. J. Mater. Eng. Perform. 2023, 33, 166-172.
- [8] Alkan, S.; Günen, A.; Gülen, M.; Gök, M.S. Effect of boriding on tribocorrosion behavior of HSLA offshore mooring chain steel. Surf. Coat. Technol. 2024, 476, 130276.
- [9] Genel, K. Boriding Kinetics of H13 Steel. Vacuum 2005, 80, 451-457.
- [10] Su, Z.G.; Lv, X.X.; An, J.; Yang, Y.L.; Sun, S.J. Role of RE Element Nd on Boronizing Kinetics of Steels. J. Mater. Eng. Perform. 2011, 21, 1337-1345.
- [11] Eyre, T.S. Brunel University Effect of Boronizing on Friction and Wear of Ferrous Metals; Elsevier Sequoia S.A.: Amsterdam, The Netherlands, 1975; Volume 34, pp. 383–397.
- [12] Mei, S.; Zhang, Y.; Zheng, Q.; Fan, Y.; Lygdenov, B.; Guryev, A. Compound Boronizing and Its Kinetics Analysis for H13 Steel with Rare Earth CeO2 and Cr2O3. Appl. Sci. 2022, 12, 3636.

- [13] Yilmaz, S.O.; Teker, T.; Karataş, S. Wear Behavior of Iron Boride Coating on AISI 4140. Prot. Met. Phys. Chem. Surf. 2016, 52, 119-127.
- [14] Orihel, P.; Drienovský, M.; Gabalcová, Z.; Jurči, P.; Keddam, M. Characterization and Boron Diffusion Kinetics on the Surface-Hardened Layers of Royalloy Steel. Coatings 2023, 13, 113.
- [15] Martini, C.; Palombarini, G.; Carbucicchio, M. Mechanism of Thermochemical Growth of Iron Borides on Iron. J. Mater. Sci. 2004, 39, 933-937.
- [16] Orihel, P.; Jurči, P.; Keddam, M. Characterizations and Kinetic Modelling of Boride Layers on Bohler K190 Steel. Coatings 2023, 13, 1000.
- [17] Kulka, M.; Makuch, N.; Piasecki, A. Nanomechanical Characterization and Fracture Toughness of FeB and Fe2B Iron Borides Produced by Gas Boriding of Armco Iron. Surf. Coat. Technol. 2017, 325, 515-532.

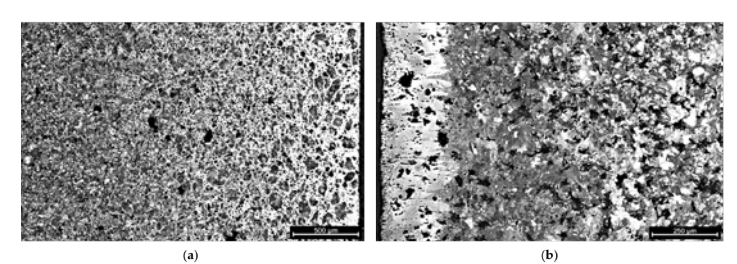


Figure 18: Microstructure of material PM1, (a) nitrided, (b) boronized; etched 2% Nital.

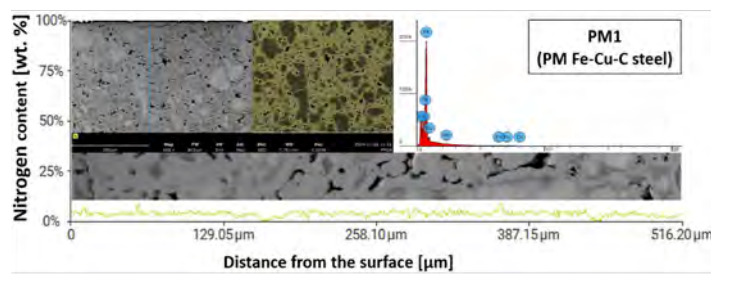


Figure 19: EDX analysis of nitriding layer in PM1 steel.

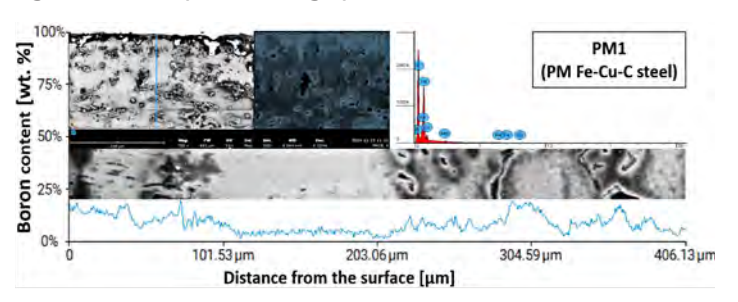


Figure 20: EDX analysis of boronizing layer in PM1 steel.

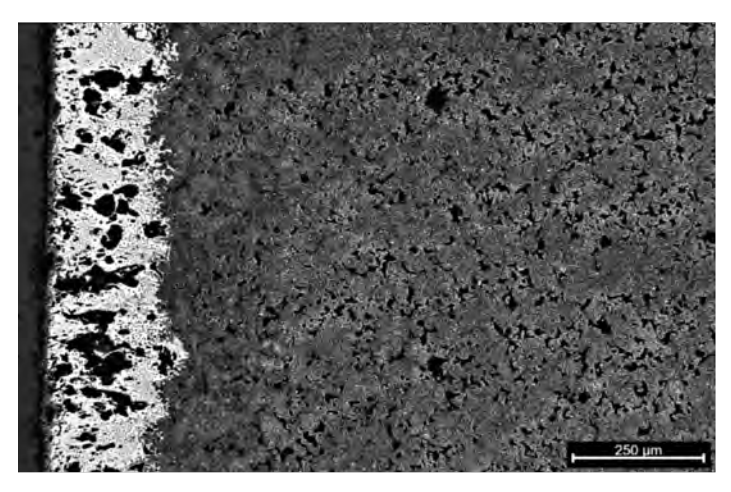


Figure 21: Microstructure of boronized PM1steel after following hardening and tempering; etched 2% Nital.

- [18] Kusmanov, S.A.; Tambovskiy, I.V.; Naumov, A.R.; Dyakov, I.G.; Belkin, P.N. Anode Plasma Electrolytic Boronitrocarburising of Low-Carbon Steel. Surf. Eng. Appl. Electrochem. 2015, 51, 462-467.
- [19] Martini, C.; Palombarini, G.; Poli, G.; Prandstraller, D. Sliding and Abrasive Wear Behaviour of Boride Coatings. Wear 2003, 256, 608-613.

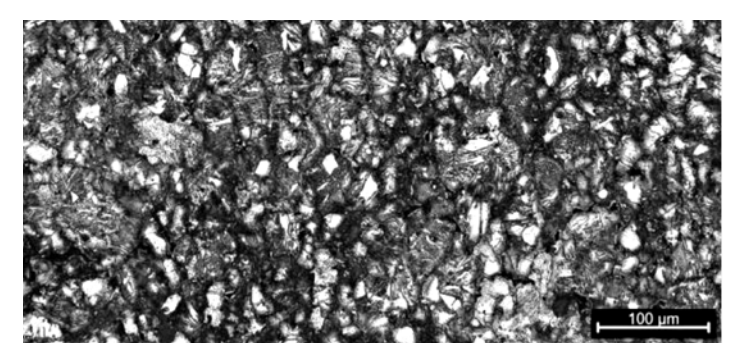


Figure 22: Basic microstructure of the PM2 steel, etched 2% Nital.

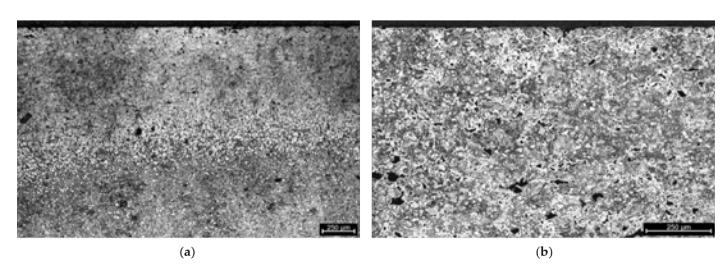


Figure 23: Microstructure of the PM2 steel, (a) induction hardened, (b) nitrided; etched 2% Nital.

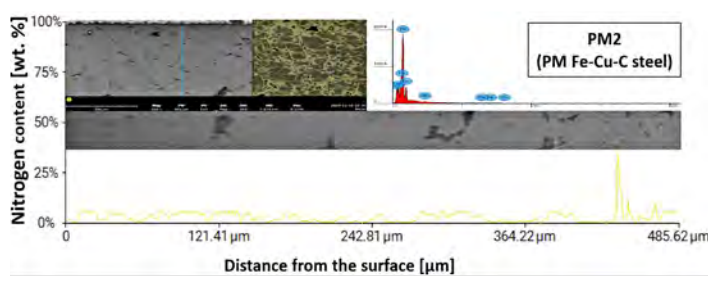


Figure 24: EDX analysis of nitriding layer in PM2 steel.

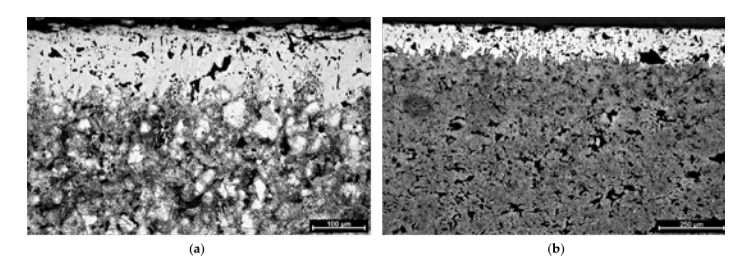


Figure 25: Microstructure of PM2 steel, (a) boronized, (b) boronized and re-hardened; etched 2% Nital.

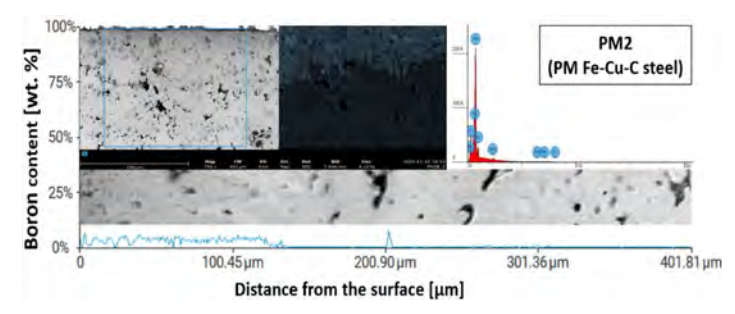


Figure 26: EDX analysis of boronising layer in PM2 steel.

- [20] Lou, D.C.; Akselsen, O.M.; Onsøien, M.I.; Solberg, J.K.; Berget, J. Surface Modification of Steel and Cast Iron to Improve Corrosion Resistance in Molten Aluminium. Surf. Coat. Technol. 2005, 200, 5282–5288.
- [21] Sireli, G.K.; Bora, A.S.; Timur, S. Evaluating the Mechanical Behavior of Electrochemically Borided Low-Carbon Steel. Surf. Coat. Technol. 2019, 381, 125177.
- [22] Chino-Ulloa, A.; Hernandes-Alejandro, M.; Castrejón-Flores, J.L.; Cabrera-González, M.; Torres-Avila, I.P.; Velázquez, J.C.; Ruiz-Trabolsi, P.A.; Hernández-Sánchez, E. Development of Ultra-Low Friction Coefficient Films and Their Effect on the Biocompatibility of Biomedical Steel. Mater. Trans. 2019, 60, 1605-1613.
- [23] Karakaş, M.S. Tribocorrosion behavior of surface-modified AISI D2 steel. Surf. Coat. Technol. 2020. 394. 125884.
- [24] Vicen, M.; Bokůvka, O.; Nikolić, R.; Bronček, J. Tribological behavior of lowalloyed steel after nitriding. Prod. Eng. Arch. 2020, 26, 78–83.
- [25] Schaefer, D.; Trombino, C. State of the North American P/M Industry 2005. Int. J. Powder Metall. 2005, 48, 27-32.
- [26] European Steel and Alloy Grades, steelnumber.com. Available online: https://www.steelnumber.com/en/steel_composition_eu.php?name_id=335 (accessed on 14 October 2024).
- [27] European Steel and Alloy Grades, steelnumber.com. Available online: https://www.steelnumber.com/en/steel_composition_eu.php?name_id=859 (accessed on 14 October 2024).
- [28] MFIP Standard 35—Materials Standards for PM Structural Parts, Standard by Metal Powder Industries Federation, 105 College Road East Princeton, New Jersey 08540-6692, USA, Published: 2024, Number of Pages: 112, ISBN 978-1-943694-41-9. Available online: https://store.accuristech.com/mpif/standards/mpif-standard-35-structural-parts?product_id=2576471#jumps (accessed on 14 October 2024).
- [29] Marucci, M.; Hanejko, F. Effect of Copper Alloy Addition Method on the Dimensional Response of Sintered Fe-Cu-C Steels. In Advances in Powder Metallurgy and Particulate Materials-2010; Bulger, M., Stebick, B., Eds.; Metal Powders Industry Federation: Princeton, NJ, USA, 2010; Part 7; pp. 11-21.
- [30] Cristofolini, I.; Pilla, M.; Molinari, A.; Menapace, C.; Larson, M. DOE Investigation of Anisotropic Dimensional Change During Sintering of Iron-Copper-Carbon. Int. J. Powder Metall. 2012, 48, 33-44.

ABOUT THE AUTHORS

František Nový, Jakub Harvanec, and Miloš Mičian are with the Faculty of Mechanical Engineering, University of Žilina in Slovakia. © 2024 by the authors. Licensee MDPI, Basel, Switzerland. This article (https://www.mdpi.com/2079-6412/14/12/1602) is an open access article distributed under the terms and conditions of the Creative Commons Attribution (CC BY) license (https://creativecommons.org/licenses/by/4.0/). It has been edited to conform to the style of Thermal Processing magazine. The statements, opinions and data contained in all publications are solely those of the individual author(s) and contributor(s) and not of MDPI and/or the editor(s). MDPI and/or the editor(s) disclaim responsibility for any injury to people or property resulting from any ideas, methods, instructions or products referred to in the content.